A Theoretical Study on the Kinetics of Hydrogen Abstraction Reactions of Methyl or Hydroxyl Radicals with Hydrogen Sulfide

S. Hosein Mousavipour,* Mohammad A. Namdar-Ghanbari, and Lila Sadeghian

Department of Chemistry, College of Sciences, Shiraz University, Shiraz, Iran

Received: October 22, 2002; In Final Form: February 11, 2003

Hydrogen abstraction reactions of methyl radicals or hydroxyl radicals with hydrogen sulfide are studied over the temperature range of 200−3000 K from a theoretical point of view. Potential energy surfaces are explored at the MP2/6-311++G(d,p) level. Values of 17.5 and 4.2 kJ mol^{-1} were found for the barrier height of reaction $CH_3 + H_2S$ at the MP4 = full/6-311++G(3df,3pd) level and of reaction $OH + H_2S$ at the QCISD = full/aug-cc-pvtz level, respectively. Rate constants of the two reactions are calculated according to generalized transition-state theory and also canonical variational transition-state theory (CVTST). According to generalized transition-state theory, both reactions showed non-Arrhenius behavior at lower and higher temperatures. The tunneling factors for both reactions are calculated at different temperatures. Characteristic tunneling temperature for reactions $CH_3 + H_2S$ and $OH + H_2S$ were found to equal 277 and 340 K, respectively. The full width of the barrier at half its height ($\Delta s_{1/2}$) were found to equal 0.37 and 0.14 Å for reaction of hydrogen sulfide with CH_3 or OH, respectively. According to CVTST, we have found the Arrhenius parameters for the reaction of $CH_3 + H_2S$, $k_1 = 6.8 \times 10^4\ T^{1.2} \exp(-6.0\ \text{kJ mol}^{-1}/(RT))$ L mol^{-1} s^{-1}, and for the reaction of $OH + H_2S$, $k_2 = 9.7 \times 10^9 \exp(-4.5\ \text{kJ mol}^{-1}/(RT))$ L mol^{-1} s^{-1}.

Introduction

Hydrogen sulfide is one of the sulfur compounds that plays an important role in the chemistry of the stratosphere. Reaction of hydrogen sulfide with different molecules and radicals in the stratosphere was the subject of many studies. For example, H_2S reacts with ozone to produce SO_2 and H_2O, which potentially is one of the sources for acidic rains.[1] Normally, reaction of H_2S with radicals is a hydrogen transfer reaction. Reaction of H_2S with different radicals such as CH_3 and OH produces SH radical, which could react with ozone in the stratosphere.[2]

$$CH_3 + H_2S \rightarrow CH_4 + SH \qquad \text{(R1)}$$

$$OH + H_2S \rightarrow H_2O + SH \qquad \text{(R2)}$$

Both CH_3 and OH radicals are important constituents in the chemistry of the stratosphere and combustion. These radicals react with most organic compounds found in the atmosphere or flame. A great deal of effort has been spent to determine the kinetic parameters for reactions in which these radicals are involved.

To the best of our knowledge, neither of the reactions R1 and R2 have so far been studied theoretically. Table 1 shows the kinetic parameters reported for reactions R1 and R2 in the literature. As shown in Table 1, the reactions have not been studied experimentally over a wide range of temperatures. Therefore, it is not possible to explore the effect of tunneling process and low-lying vibrational states on the curvature of Arrhenius plots of these reactions from the experimental results. In the present work, the rate constants of reactions R1 and R2 are calculated and the cause(s) for the possible non-Arrhenius behavior of both reactions is investigated. Thus, high-level ab initio calculations are carried out to acquire the potential energy surfaces for both reactions, and their rate constants are calculated theoretically according to generalized transition-state theory and canonical variational transition-state theory (CVTST) over the temperature range of 200−3000 K.

TABLE 1: Arrhenius Parameters Reported for Reactions R1 and R2 in the Literature

A (L mol^{-1} s^{-1})	n	E_a (kJ mol^{-1})	T (K)	ref
		$CH_3 + H_2S$		
1.26×10^8		9.6	743−772	3
1.38×10^8		9.2	332−432	4
3.80×10^8		10.9	350−600	5
5.01×10^7		12.1	372−444	6
3.16×10^8		11.1	473−573	7
2.51×10^8		10.9	323−473	8
		$OH + H_2S$		
3.61×10^9		0.6	200−300	2a
3.67×10^9		0.7	220−520	2b
2.71×10^9			298−885	9
7.94×10^9		3.3	243−363	10
3.13×10^9			300	11
229.0	2.43	−6.1	245−450	12
3.13×10^9			300	13
3.02×10^9			228−437	14
4.70×10^9		1.2	239−425	15
3.56×10^9		0.7	228−518	16
3.85×10^9		0.4	244−367	17
3.01×10^9			297	18
3.13×10^9			297−427	19
1.87×10^9			298	20
1.40×10^{10}		3.7	298−885	21

Different reasons might cause a curved Arrhenius plot. One being the nonlinearity of Arrhenius plot of hydrogen transfer reactions is quantum mechanical tunneling effect, which is important at lower temperatures. The other reasons for nonlinearity of Arrhenius plot are low-lying vibrational states or low-lying electronic states, of which the effects appear at higher temperatures where low-lying states are populated. In the present work, the rate constants of reactions R1 and R2 are calculated by means of generalized transition-state theory and the extent

10.1021/jp022291z CCC: $25.00
Published on Web 04/11/2003

of the role of tunneling and low vibrational frequencies on the nonlinearity of Arrhenius plots is explored. Also, the rate constants are calculated according to CVTST to diminish the curvature of Arrhenius plot caused by low-lying vibrational states. The characteristic tunneling temperature and full width of barrier at half its height for both reactions are also calculated.

Ab Initio Calculations

The Gaussian W98[22] program is used to carry out quantum chemical calculations. Potential energy surfaces along the minimum energy paths for reactions R1 and R2 were explored at the MP2/6-311++G(d,p) level. Geometries of reactants, transition states, and products were optimized at the MP2/6-311++G(3df,3pd) level of theory. Spin contamination was annihilated by using the PUMP2 energies.[23] The location of the transition state along the reaction path was searched manually and also by QST2 method utilized in the Gaussian W98 program. These two methods gave almost the same position and geometry for the transition states of both reactions R1 and R2. Frequencies of activated complexes were calculated at the MP2/6-311G(d,p) level and scaled by a factor of 0.95.[24] There was only one imaginary frequency for the transition states.

Single-point MP4SDTQ[25] calculations on the MP2 geometries were carried out to obtain more accurate energies along the reaction coordinate. To compare the ability of different methods to predict the energies, CASMP2,[26] QCISD,[27] CCSD,[26] and DFT (with Becke's three-parameter hybrid functional B3LYP)[28] calculations with more flexible basis set 6-311++G(3df,3pd) were also performed. Attempts were made to minimize the calculated barrier height of reaction R2 by performing the QCISD = full/aug-cc-pvtz calculations. MP2 geometries were used in CASMP2, CCSD, and QCISD calculations, while in the DFT calculations the stationary points were reoptimized at the B3LYP/6-311G(d,p) level.

Calculation of Rate Constants

The general expression for generalized transition-state theory is as follows:[29,30]

$$k(T) = \Gamma \frac{k_B T}{h} \sigma \frac{Q^{\ddagger}}{Q_A Q_B} \exp\left(-\frac{V_{MEP}(s)}{k_B T}\right) \quad (1)$$

Here k_B and h are Boltzmann's and Planck's constants, respectively, Γ is the tunneling factor, σ is the reaction path degeneracy (the ratio of symmetry numbers from the rotational partition functions), the Q parameters are the product of translational, rotational, vibrational, and electronic partition functions for the transition state (numerator) and reactants (denominator), and s is the distance along the reaction path from the saddle point. The reaction path is generally taken to be the minimum energy path (MEP) from the saddle point to the reactant and product geometries.[31] V_{MEP} is the value of potential energy corrected for zero-point energy at the generalized transition-state theory. To show the influence of a possible tunneling process on the curvature of the Arrhenius plot at lower temperatures, calculations were carried out by including and excluding the tunneling factor.

Canonical variational transition-state theory[32] was also applied on the assumption that conserved vibrational frequencies and moments of inertia of the fragments do not change during the course of reaction. The method of calculations is described in ref 32a.

A careful investigation was done to follow the changes, which may occur in different degrees of freedom as reactions proceed. The translational partition function per unit volume of a molecule of mass m in three dimensions is

$$Q_{tr} = \left(\frac{2\pi m k_B T}{h^2}\right)^{3/2} \quad (2)$$

The external rotational partition function for a nonlinear molecule has the following form:

$$Q_{rot} = \frac{8\pi^2 (8\pi^3 I_a I_b I_c)^{1/2} (k_B T)^{3/2}}{\sigma h^3} \quad (3)$$

Here, the I parameters are the moments of inertia and σ is a symmetry number. As two reactants approach each other, three (for nonlinear molecules) or two (for linear molecules) external rotations would transform to hindered rotations or harmonic vibrations as they approach the transition state. One of those rotations is the rotation around the reaction coordinate axis, which could be treated as a vibrational motion or an internal rotation. The partition function for this kind of internal rotation might be written as

$$Q_{rot} = \frac{(2\pi)^{1.5} (I_{IR} k_B T)^{0.5}}{\sigma_x h} \quad (4)$$

Here, I_{IR} is the reduced moment of inertia. To calculate the reduced moment of inertia for this internal rotation, we used a FORTRAN program based on the method introduced by Pitzer.[33]

The other two rotations around the axes perpendicular to the reaction coordinate axis would transform to two-dimensional hindered internal rotations as the transition state is approaching. These two motions usually are considered as rocking or tumbling vibrational motions in molecules. The partition function for this kind of hindered rotations is difficult to calculate. In the limit of high temperatures or low barriers for rotation, LeBlance and Pacey suggested the partition function for a two-dimensional hindered rotor as[34]

$$Q_{hin} = \left(\frac{I_{IR} k_B T}{\eta^2}\right) \exp\left(\frac{E^0 - V}{k_B T}\right) \quad (5)$$

Here I_{IR} is the reduced moment of inertia for the hindered rotation, E^0 is the zero-point energy for this degree of freedom, and V is two-thirds the height of the barrier to rotation. The value of V might be calculated from the related bending frequency as[35]

$$V = {}^4/_3 I(\pi\nu)^2 \quad (6)$$

Here, ν is the term value for the rocking or tumbling motion.

Pitt, Gilbert, and Ryan introduced a hindered rotational constant B_{eff} ($2B_{free}/(1 - \cos\theta_{hin})$) to calculate hindered rotation partition function.[36] They rewrote eq 4 as

$$Q_{hin} = \left(\frac{\pi k_B T}{B_{hin}}\right)^{1/2} \quad (7)$$

Here, θ_{hin} is the average hindrance angle and could vary from 0 to $\pi/2$. B_{free} is the rotational constant of the corresponding two-dimensional free rotor. When separation of reactants is longer than the critical distance, $\theta_{hin} = 90$, then $B_{eff} = 2B_{free}$.

Vibrations in the transition state are usually treated as harmonic oscillators and occasionally as hindered rotations. The

vibrational partition function for one degree of freedom is calculated as

$$Q_v = \frac{1}{1 - e^{-h\nu/(k_B T)}} \quad (8)$$

The number of bending motions (low frequencies) is different in reactants, transition state, and products. At high temperatures, when $T \gg \theta$ ($\theta = h\nu/k_B$), the vibrational partition function may be approximated by expanding the exponential term as $Q_v = k_B T/(h\nu)$, which causes an increase of the sensitivity of the preexponential factor to temperature.

Tunneling Factor

According to classical mechanics, a particle can cross a potential energy barrier only if its energy is higher than the barrier height, while quantum mechanics predicts that there is a probability for the crossing at lower particle energies. This transmission probability is very sensitive to the particle energy and mass, the barrier height, and the shape of the barrier.[37]

The tunneling correction factor is defined as the quotient of the quantum mechanical rate to the classical rate. Although the tunneling process is a multidimensional phenomenon, for simplicity this is treated as a one-dimensional process. In this study, two methods were considered for the correction of possible tunneling effect. A simple expression, which is suggested by Shavitt for the tunneling correction, is[38]

$$Q_{tunnel} = 1 - \frac{1}{24}\left(\frac{h\nu^*}{k_B T}\right)^2 \left(1 + \frac{k_B T}{E_0}\right) \quad (9)$$

where ν^* is the imaginary frequency of the activated complex at the top of the barrier, k_B and h are Boltzmann's and Plank's constants, and E_0 is the barrier height corrected for zero-point energy for the reaction. In another method to calculate the tunneling factor, a particle with energy of E approaching an unsymmetrical Eckart barrier is assumed.[39] In this method, the tunneling factor can be written as[40]

$$\Gamma = \exp(E_e/(k_B T)) \int_0^\infty \kappa(E) \exp(-E/(k_B T))\, dE/(k_B T) \quad (10)$$

Here E_e is the effective barrier height corrected for zero-point energies, and $\kappa(E)$ is the transmission probability for a particle with energy E approaching an Eckart barrier. To calculate the tunneling factor, a numerical integration program of Brown was used.[41] The tunneling factor, Γ, in expression 10 is related to the barrier heights for forward and reverse reaction and frequency of an imaginary vibration, ν^*, in a well created by inverting the barrier. To calculate the tunneling factor according to eq 10, three parameters, α_i ($2\pi V_i/(h\nu^*)$ where i is 1 or 2 for forward or reverse reaction) and u^* ($h\nu^*/(k_B T)$) should be introduced to the program as input. At the characteristic tunneling temperature, T^* ($h\nu^*/(2\pi k_B)$), the energy of the reacting molecules is equal to half the effective barrier, E_e. The full width of a parabolic barrier at half its height ($\Delta s_{1/2}$) is related to the characteristic tunneling temperature as[42]

$$\Delta s_{1/2} = \frac{h E_e^{1/2}}{2\pi^2 k_B T^* \mu^{1/2}} \quad (11)$$

Here k_B and h are Boltzmann's and Planck's constants, respectively, E_e is the barrier height, and μ is the reduced mass of the transient species in the direction of reaction coordinate.

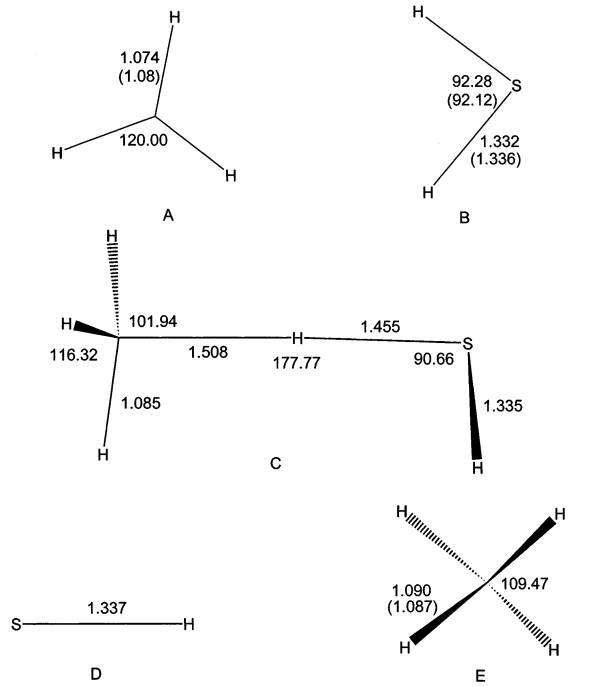

Figure 1. Optimized structures of CH_3 (A), SH_2 (B), TS1 (C), SH (D), and CH_4 (E) at the MP2/6-311++G (3df,3pd) level. Numbers in parentheses are from ref 43.

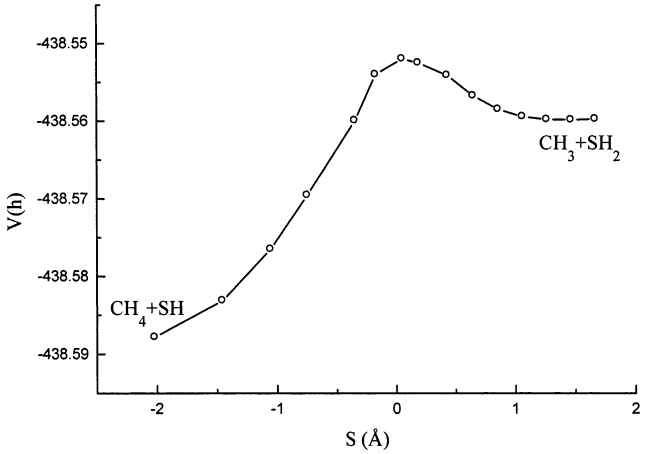

Figure 2. Potential energy surface for reaction $CH_3 + H_2S$ at the MP2/6-311++G(d,p) level.

μ in reactions R1 and R2 is taken as the mass of a hydrogen atom that passes through the barrier.

Results and Discussion

a. Reaction of $CH_3 + H_2S$. Figure 1 shows the geometry of optimized structures of species in reaction R1 at the MP2/6-311++G(3df,3pd) level of theory. Numbers in parentheses are experimental values given in ref 43. As shown in Figure 1c, the location of the transition state for reaction R1 was found at C···H distance of 1.508 Å and H···S distance of 1.455 Å. The angle of C···H···S at the transition state was found equal to 177.77°. These results are in agreement with the results reported for some other hydrogen abstraction reactions.[40,44] Figure 2 shows the potential energy surface along the minimum energy path for reaction R1 at the MP2/6-311++G(d,p) level of theory. According to Figure 2, reaction R1 is an exothermic reaction with an early barrier. Total energies of species at different levels of theory are listed in Table 2. The barrier heights corrected for zero-point energies at different levels of theory are listed in Table 3. Vibrational term values, rotational constants, reduced

TABLE 2: Total Energies of Species in Reaction $CH_3 + H_2S$ Calculated at Different Levels of Theory in amu

method	CH_3	H_2S	$CH_3\cdots SH_2$[a]	TS	HS	CH_4
(P)MP2 = full/6-311++(3df,3pd)	−39.759 74	−399.066 70	−438.826 44	−438.822 95	−398.418 83	−40.433 95
MP4SDTQ = full/6-311++(3df,3pd)	−39.782 76	−399.096 47	−438.879 23	−438.873 42	−398.444 85	−40.460 97
QCISD = full/6-311++(3df,3pd)	−39.779 12	−399.087 73	−438.866 85	−438.859 03	−398.438 64	−40.455 11
CCSD = full/6-311++(3df,3pd)	−39.778 96	−399.087 50	−438.866 46	−438.858 45	−398.438 45	−40.454 81
B3LYP/6-311++(3df,3pd)	−39.858 33	−399.429 69	−439.288 02	−439.285 45	−398.777 65	−40.537 39
CAS(MP2)/6-311++(3df,3pd)	−39.760 27	−399.043 34	−438.803 61		−398.324 88	−40.427 89

[a] Sum of total energies of CH_3 plus H_2S at an infinite distance.

TABLE 3: Barrier Height Corrected for Zero-Point Energies for Reaction R1 at Different Levels of Theory in kJ mol^{-1}

method of calculation	E_0
(P)MP2 = full/6-311++G(3df,3pd)	11.5
MP4SDTQ = full/6-311++G(3df,3pd)	17.5
CASMP2/6-311++G(3df,3pd)	
B3LYP/6-311++G(3df,3pd)	9.0
QCISD = full/6-311++G(3df,3pd)	22.8
CCSD = full/6-311++G(3df,3pd)	23.3

TABLE 4: Vibrational Term Values in cm^{-1}, Zero-Point Energies in amu, and Rotational Constants in GHz Calculated at the MP2/6-311G(d,p) Level and Reduced Moments of Inertia, I_{IR}, in kg mol^{-1} Å^2 for the Transition State (See the Text)

	CH_3	SH_2	TS
ν	3161, 3161, 3004, 1396, 1396, 606	2626, 2615, 1183	3309 (3143), 3306 (3141), 3134 (2977), 2811 (2670), 1453 (1380), 1453 (1380), 1229 (1168), 1162 (1104), 825 (784), 647 (615), 571 (542), 316 (300), 280 (266), 38 (36), 1209i
B1	289.661	311.005	97.821
B2	289.661	269.543	5.306
B3	144.830	141.862	5.211
I_{IR}			1.14, 0.90, 0.84
ZPE	0.030 25	0.015 71	0.046 82

moments of inertia, and zero-point energies for reaction R1 are listed in Table 4. Vibrational term values for CH_3 and H_2S are from refs 45 and 46, respectively. Reaction R1 has an early energy barrier with an imaginary term value of 1209i cm^{-1}. This low imaginary term value causes a lower characteristic tunneling temperature of 277 K relative to the values reported for some other hydrogen transfer reactions.[47] The full width of the barrier at half its height ($\Delta s_{1/2}$) for reaction R1 from eq 11 was calculated to equal 0.37 Å, which is almost half the value obtained from Figure 2.

Comparing the calculated barrier height for reaction R1 at different levels of theory in the present work with the reported experimental values of barrier height in the literature reveals that our results show a higher barrier height. Reported experimental barrier heights in the literature vary from 9 to 11 kJ mol^{-1} (see Table 1). To calculate the rate constant k_1 in the present study, we chose a barrier height equal to 17.5 kJ mol^{-1} from MP4SDTQ results.

Rate constant for reaction R1 was calculated according to generalized transition-state theory, eq 1, and also CVTST; the methods of calculation are described in ref 32a. Reaction path degeneracy for reaction R1 was set equal to 4. A value of 1 was chosen for the quotient of electronic partition functions. The Arrhenius plot for reaction R1 is shown in Figure 3. To calculate the rate constant for reaction R1, the rotation of the coming CH_3 group about the C···H···S bond at the transition state could be treated as a vibrational motion or an internal rotation. Also the rotations of CH_3 group around the two axes perpendicular to the reaction coordinate axis could be treated as rocking or tumbling vibrational motions or two hindered

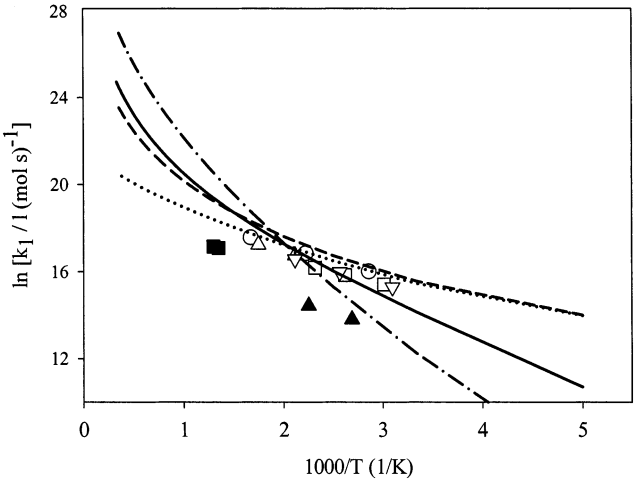

Figure 3. Arrhenius plot for reaction $CH_3 + H_2S$. Solid line is calculated according to eq 1 without introducing the tunneling correction. Dashed line is the same as solid line except that the tunneling factor is included. Dashed−dotted line is the same as the dashed line except that the three vibrational motions in the transition state are treated as three internal rotations. Dotted line is calculated according to CVTST method. Symbols represent data from the following references: (■) ref 3; (□) ref 4; (○) ref 5; (▲) ref 6; (△) ref 7; (▽) ref 8.

internal rotations. The rotation of CH_3 group around the reaction coordinate (torsional motion) was treated as an internal free rotation, and we used eq 4 to calculate the partition function for this free rotation. We used a FORTRAN program based on the method introduced by Pitzer[33] to calculate the reduced moment of inertia in eq 4. We obtained a value of 1.14 amu Å^2 for I_{IR} for this rotation. To calculate the partition function for the hindered rotations about the axes perpendicular to the reaction coordinate, we used eq 5. The reduced moment of inertia in eq 5 was calculated as[48]

$$I_{IR} = \frac{I_1 I_2}{I_1 + I_2} \tag{12}$$

Here, I_1 and I_2 are the moments of inertia of the two parts. We found values of I_{IR} for these rotations of 0.84 and 0.90 amu Å^2.

In calculating the solid line in Figure 3, we treated these three motions of CH_3 group as vibrational motions with no tunneling correction, eq 1. The dashed line in Figure 3 is the same as the solid line except that the tunneling correction, eq 10, was included. The dashed−dotted line in Figure 3 is the same as the dashed line except that the three internal motions of CH_3 group about the *X*, *Y*, and *Z* axes were treated as internal rotations in the transition state. The dotted line in Figure 3 was calculated according to the assumption that conserved vibrational frequencies and moments of inertia of the reactants do not change as the reaction proceeds. To calculate the dotted line in Figure 3, the free internal rotation and tumbling and rocking motions are considered and the tunneling factor was also included. According to CVTST, the dotted line in Figure 3, we have found the Arrhenius parameters for the reaction of

TABLE 5: Total Energies of Species in Reaction OH + H_2S Calculated at Different Levels of Theory in amu

method	OH	H_2S	HO−H−SH[a]	TS	H_2O	HS
(P)MP2 = full/6-311++G(3df,3pd)	−75.645 35	−399.066 70	−474.712 05	−474.711 20	−76.347 63	−398.418 83
MP4SDTQ = full/6-311++G(3df,3pd)	−75.662 31	−399.096 47	−474.758 78	−474.755 72	−76.362 60	−398.444 85
QCISD = full/6-311++G(3df,3pd)	−75.657 53	−399.087 73	−474.745 26	−474.742 32	−76.353 31	−398.438 64
QCISD = full/aug-cc-pvtz	−75.653 40	−398.970 03	−474.623 43	−474.622 13	−76.349 14	−398.320 25
CCSD = full/6-311++G(3df,3pd)	−75.657 22	−399.087 50	−474.744 72	−474.740 91	−76.352 84	−398.438 45
B3LYP/6-311++G(3df,3pd)	−75.766 22	−399.429 69	−475.195 91	−475.204 15	−76.464 44	−398.777 65
CAS(MP2)/6-311++G(d,p)	−75.591 64	−398.946 47	−474.538 12		−76.281 85	−398.321 03

[a] Sum of total energies of OH plus H_2S at an infinite distance.

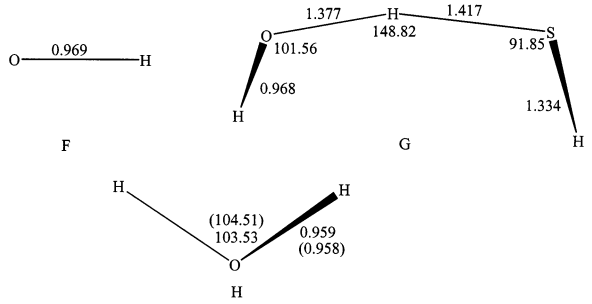

Figure 4. Optimized structure of OH (F), TS2 (G), and H_2O (H) at the MP2/6-311++G(3df,3pd) level. Numbers in parentheses are from ref 43.

$CH_3 + H_2S$ as $k_1 = (6.8 \times 10^4)T^{1.2} \exp(-6.0 \text{ kJ mol}^{-1}/(RT))$ L mol^{-1} s^{-1}.

Equation 10 was used to calculate the tunneling factor in Figure 3. The tunneling factor for reaction R1 was found equal to 3.9 at 300 K, which decreased to a value of 1.16 at 1000 K. The calculated tunneling factor for reaction R1 according to eq 9 was found to equal 2.60 at 300 K. In Figure 3, our results are compared with the experimental results reported in the literature.

We also assumed the tumbling and rocking motions of CH_3 as two-dimensional hindered rotations as the transition state is approaching and calculated their partition functions by means of eqs 5 or 7. At the transition state, term values for the internal rotation around the reaction coordinate and tumbling and rocking motions were found to equal 36, 266, and 300 cm^{-1}, respectively; see Table 4. Using eq 4 to calculate the partition function for the internal rotation about the reaction coordinate axis and eq 5 to calculate the partition function for the other two-dimensional hindered rotations produced the rate constant of reaction R1 with much higher slope (see the dashed−dotted line in Figure 3).

Reaction R1 is an exothermic reaction with an early barrier. Values of $\Delta_f H^0$ for CH_3, CH_4, HS,[49] and H_2S[50] are reported as 146.3 ± 0.5, −74.6 ± 0.3, 140.4 ± 3.5, and −20.6 ± 0.5 kJ mol^{-1}, respectively, at 298 K. According to these data, ΔH^0 for reaction R1 was found to equal −60 ± 4 kJ mol^{-1} at 298 K. According to our MP2/6-311G(d,p) calculations, ΔH^0 for reaction R1 was found to be −66.3 kJ mol^{-1} at 298 K, which seems reasonable.

b. Reaction of OH + H_2S. Optimized geometries of OH radical, transition state, and H_2O at the MP2/6-311++G-(3df,3pd) level are shown in Figure 4. Potential energy surface for reaction R2 at the MP2/6-311G++(d,p) level is shown in Figure 5. The location of the transition state for reaction R2 was found at O···H distance of 1.377 Å and at H···S distance of 1.417 Å. The angle of C···H···S at the transition state was found to equal 148.82°. This value could be compared with the value of 148° reported by Corchado et al. for reaction of OH + NH_3.[51] Total energies of species at different levels of theory are listed in Table 5. The barrier heights corrected for zero-point energies at different levels of theory are listed in Table 6. Vibrational term values, rotational constants, reduced moments of inertia, and zero-point energies for reaction R2 are listed in Table 7. Depending on the level of theory, the calculated barrier heights for reaction R2 were found in the range from −20.8 to 10.8 kJ mol^{-1}. DFT methods gave no barrier height for reaction R2. We chose a value of 4.2 kJ mol^{-1} for the barrier height of reaction R2 from QCISD = full/aug-cc-pvtz calculations.

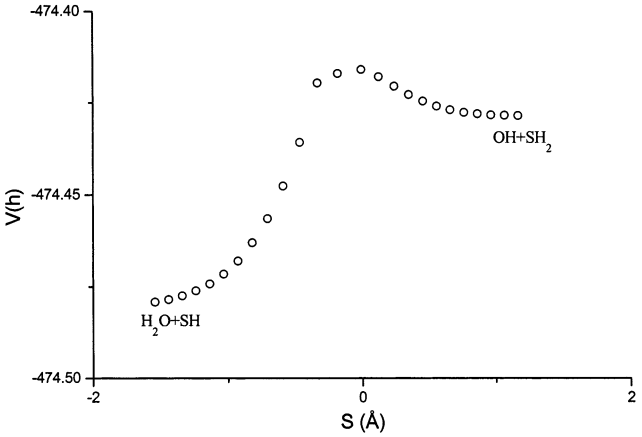

Figure 5. Potential energy surface for reacton OH + H_2S at the MP2/6-311++G(d,p) level.

TABLE 6: Barrier Height Corrected for Zero-Point Energies for Reaction R2 at Different Levels of Theory in kJ mol^{-1}

method of calculation	E_0
(P)MP2 = full/6-311++G(3df,3pd)	3.0
MP4SDTQ = full/6-311++G(3df,3pd)	8.8
CASMP2/6-311++G(d,p)	
B3LYP/6-311++G(3df,3pd)	−20.8
QCISD = full/6-311++G(3df,3pd)	8.5
QCISD = full/aug-cc-pvtz	4.2
CCSD = full/6-311++G(3df,3pd)	10.8

TABLE 7: Vibrational Term Values in cm^{-1}, Zero-Point Energies in amu, and Rotational Constants in GHz Calculated at the MP2/6-311G(d,p) Level and Reduced Moments of Inertia, I_{IR}, in kg mol^{-1} Å^2 for the Transition State (See the Text)

	H_2S	OH	TS
ν	2626, 2615, 1183	3737.8	3839 (3647), 2824 (2683), 1409 (1339), 1093 (1039), 772 (733), 340 (323), 275 (262), 210 (200), 1487i
B1	311.104	568.336	181.436
B2	272.012	568.336	6.147
B3	145.124		6.077
I_{IR}			0.41, 0.57
ZPE	0.015 71	0.008 52	0.024 52

Reaction R2 is also an exothermic reaction with an early barrier. Using values of 39.4 ± 0.2 and −241.8 ± 0.1 kJ mol^{-1} for the heats of formation of hydroxyl radical[45] and water,[46] respectively, and values from the last section for the heats of formation of H_2S and HS radical, we found a value of −120 ± 4 kJ mol^{-1} for ΔH^0 of reaction R2 at 298 K. According to our

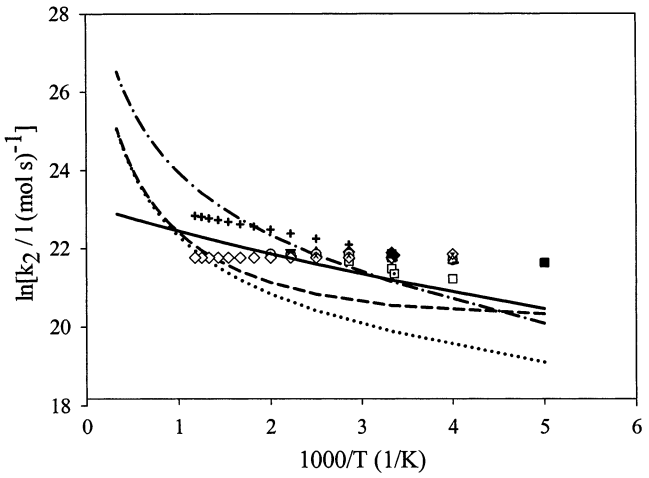

Figure 6. Arrhenius plot for reaction OH + H_2S. Dotted line is calculated from eq 1 without introducing the tunneling correction. Dashed line is the same as dotted line except that the tunneling factor is included. Dashed−dotted line is the same as dashed line except that the two vibrational motions in the transition state are treated as two internal rotations. Solid line is calculated according to CVTST method. The symbols represent data from the following references: (■) ref 2a; (□) ref 10; (○) ref 2b; (▲) ref 13; (×) ref 14; (◇) ref 9; (dotted diamond) ref 17; (▼) ref 12; (−) ref 16; (△) ref 15; (⊡) ref 20; (bold box) ref 11; (◆) ref 18; (⊙) ref 19; (+) ref 21.

MP2/6-311G(d,p) calculations, ΔH^0 for reaction R2 was found to be −119.8 kJ mol^{-1} at 298 K, which is in good agreement with the experimental results.

The term value for the imaginary frequency for reaction R2 was found to equal 1487i (see Table 7). This value of imaginary frequency predicts a value of 340 K for the characteristic tunneling temperature. The full width of the barrier at half its height ($\Delta s_{1/2}$) for reaction R2 was calculated to equal 0.14 Å using eq 11, which is smaller than the value obtained from Figure 5 by 0.45 Å.

Rate constant for reaction R2 was calculated according to eq 1. Reaction path degeneracy for reaction R2 was set equal to 2. A value of 1 was chosen for the quotient of electronic partition functions. Arrhenius plot for reaction R2 is shown in Figure 6. To calculate the rate constant for reaction R2, four different methods were used. In the first method, all of the internal motions of the system in the transition state were treated as vibrational motions with no tunneling correction (dotted line in Figure 6). In the second method, we calculated the rate constant of reaction R2 in the same way as we did for the dotted line except that the tunneling correction to the rate constant from eq 10 was included (dashed line in Figure 6). In the third method, we treated the tumbling and rocking motions and free rotation about the reaction coordinate in the activated complex as internal rotation and calculated the partition functions for these rotations by means of eqs 4 and 5 (dashed−dotted line in Figure 6). We obtained a value of 0.41 amu Å^2 for the reduced moment of inertia for the internal rotation of hydrogen of hydroxyl radical around the S···H···O axis and a value of 0.57 amu Å^2 for the reduced moment of inertia for the hindered internal rotation of hydroxyl group around the axis perpendicular to the reaction coordinate axis. At the transition state, term values for the internal rotation around the reaction coordinate and tumbling or rocking motions of OH group were found to equal 200 and 262 cm^{-1}, respectively (see Table 7). The solid line in Figure 6 was calculated according to CVTST using the method described in ref 32a. According to this method, we have found the Arrhenius parameters for the reaction of OH + H_2S as $k_2 = 9.7 \times 10^9 \exp(-4.5 \text{ kJ mol}^{-1}/(RT))$ L mol^{-1} s^{-1}.

In Figure 6, we compared our results with the reported values of the rate constant k_2 in the literature. As shown in Figure 6 and Table 1, because of low activation energy for reaction R2, the reported Arrhenius plots in the literature are almost independent of the temperature. The solid line in Figure 6 shows more agreement with the results obtained from the literature. Our calculated Arrhenius plots from generalized transition-state theory for reaction R2 were curved at higher temperatures, which was due to the contribution of low vibrational states of the transition state.

The tunneling factor calculated from eq 10 for reaction R2 was found to equal 1.96 at 300 K and decreased to a value of 1.1 at 1000 K. According to eq 9, this factor was found to equal 4.7 at 300 K.

Conclusion

Reactions R1 and R2 are hydrogen abstraction reactions, of which, as yet, the kinetics are not studied experimentally in a wide range of temperature. As expected, the rate constants of hydrogen abstraction reactions are normally affected by quantum mechanical tunneling process. This effect becomes small as the barrier height decreases. We calculated the rate constants for reactions R1 and R2 over the temperature range of 200−3000 K, theoretically. Potential energy surfaces for both reactions were explored at the MP2/6-311++G(d,p) level of theory, and barrier heights were calculated at different levels of theory. Both reactions are exothermic with early barriers. Generalized transition-state theory and canonical variational transition-state theory were used to calculate the rate constants. To calculate the rate constants for reactions R1 and R2, we used the results from MP4SDTQ and QCISD calculations, respectively, which showed more agreement with the experimental results.

DFT method gave the lowest barrier height for reaction R1, which increased the rate of reaction R1 by a factor of 30 at 300 K, while CCSD calculations gave a higher barrier, which caused a decrease of the rate of reaction R1 by 10% relative to the rate constant calculated from MP4SDTQ results at 300 K. The MCSCF method was not able to converge at the transition states of both reactions R1 and R2. The Gaussian program was also unable to converge at the transition state of reaction R1 at the QCISD = full/aug-cc-pvtz level.

DFT method gave no barrier for reaction R2. Our results showed the rate constant of reaction R2 calculated according to QCISD = full/aug-cc-pvtz results was in more agreement with the experimental results.

The effect of treating tumbling and rocking motions as hindered internal rotations on the rate constants was also examined. For both reactions, we found that the trend of the rate constants was in more agreement with the experimental results if we used these internal rotations as tumbling or rocking vibrational motions (see Figures 3 and 6).

As indicated in Table 1, reactions R1 and R2 have not been studied over a wide range of temperature experimentally. Thus, it was not possible to examine the role of tunneling process on the rates of these reactions from the experimental data reported in the literature. Our results indicated that tunneling effect on the rate of reaction R1 becomes significant at temperatures lower than 277 K and for reaction R2 at temperatures lower than 340 K. These characteristic tunneling temperatures are strongly dependent on the values of imaginary frequencies. The tunneling factor for reaction R1 was found to equal 3.90 at 300 K, which decreased to a value of 1.16 at 1000 K. The tunneling factor for reaction R2 was found to equal 1.96 at 300 K and decreased to a value of 1.1 at 1000 K. The reason for the lower tunneling factor in reaction R2 should be due to lower barrier height of reaction R2.

Our ab initio calculations gave higher barrier heights for both reactions than the values reported from experimental studies in the literature (see Table 1). This discrepancy should be due to the compensation of the tunneling effect in the experimental studies. To evaluate the effect of tunneling process in both reactions, it is necessary to study both reactions in a wider temperature range. Despite this discrepancy, if we include the tunneling factor into the rate constants, our results are in good agreement with the experimental results (see the dotted line and solid line in Figures 3 and 6, respectively).

Lin et al.[12] reported a non-Arrhenius behavior for the rate constant of reaction R2 with a minimum near room temperature. DeMore and co-workers[2a] and Atkinson and co-workers[2b] suggested that this kind of non-Arrhenius behavior is due to the occurrence of both addition and abstraction channels for the OH + H_2S system. We were not able to find a relatively stable geometry for the addition of hydroxyl radical to hydrogen sulfide. We believe that this kind of behavior should be the result of tunneling process.

As shown in Figures 3 and 6, Arrhenius plots for both reactions R1 and R2 are nonlinear at higher temperatures if we use generalized transition-state theory. This kind of behavior should be due to the contribution of low-lying vibrational states presented in the transition state. High-frequency stretching vibrations are considered to be unexcited while low-frequency bending vibrations will be excited at higher temperatures. If we assume that conserved vibrational frequencies and moments of inertia of the reactants do not change as the reactions proceed, Arrhenius plots of both reactions are in more agreement with the experimental results (see dotted line in Figure 3 and solid line in Figure 6).

According to CVTST, Arrhenius plot of reaction R1 was not linear with a small curvature (see dotted line in Figure 3). A nonlinear least-squares curve fitting to the dotted line in Figure 3 gave the Arrhenius parameters as $k_1 = (6.8 \times 10^4)T^{1.2}$ exp(−6.0 kJ mol^{-1}/(RT)) L mol^{-1} s^{-1}. CVTST calculations gave almost a linear Arrhenius plot for reaction R2 (see solid line in Figure 6) with Arrhenius parameters $k_2 = 9.7 \times 10^9$ exp(−4.5 kJ mol^{-1}/(RT)) L mol^{-1} s^{-1}. The reason for the difference in behavior of these two reactions was because the calculated tunneling factor of reaction R1 was almost two times greater than that of reaction R2.

Acknowledgment. This work was supported by the Research Council of Shiraz University.

References and Notes

(1) Glavas, S.; Toby, S. *J. Phys. Chem*. **1975**, *79*, 779.
(2) For example, see: (a) DeMore, W. B.; Sander, S. P.; Golden, D. M.; Hampson, R. F.; Kurylo, M. J.; Howard, C. J.; Ravishankara, A. R.; Kolb, C. E.; Molina, M. J. *JPL Publ.* **1997**, *97-4*, 1. (b) Atkinson, R.; Baulch, D. L.; Cox, R. A.; Hampson, R. F., Jr.; Kerr, J. A.; Rossi, M. J.; Troe, J. *J. Phys. Chem. Ref. Data* **1997**, *26*, 1329.
(3) Perrin, D.; Richard, C.; Martin, R. *J. Chim. Phys*. **1988**, *85*, 185.
(4) Arican, H.; Arthur, N. L. *Aust. J. Chem*. **1983**, *36*, 2195.
(5) Arthur, N. L.; Bell, T. N. *Rev. Chem. Intermed.* **1978**, *2*, 37.
(6) Gray, P.; Herod, A. A.; Leyshon, L. J. *Can. J. Chem*. **1969**, *47*, 689.
(7) Imai, N.; Dohmaru, T.; Toyama, O. *Bull. Chem. Soc. Jpn*. **1965**, *38*, 639.
(8) Imai, N.; Toyama, O. *Bull. Chem. Soc. Jpn*. **1960**, *33*, 652.
(9) Tyndall, G. S.; Ravishankara, A. R. *Int. J. Chem. Kinet.* **1991**, *23*, 483.
(10) Lafage, C.; Pauwels, J.-F.; Carlier, M.; Devolder, P. *J. Chem. Soc., Faraday Trans. 2* **1987**, *83*, 731.
(11) Barnes, I.; Bastian, V.; Becker, K. H.; Fink, E. H.; Nelsen, W. J. *Atmos. Chem*. **1986**, *4*, 445.
(12) Lin, Y.-L.; Wang, N.-S.; Lee, Y.-P. *Int. J. Chem. Kinet*. **1985**, *17*, 1201.
(13) Barnes, I.; Bastian, V.; Becker, K. H.; Fink, E. H. *Phys. Chem. Behav. Atmos. Pollut. Proc. Eur. Symp*. **1984**, 149.
(14) Michael, J. V.; Nava, D. F.; Brobst, W. D.; Borkowski, R. P.; Stief, L. J. *J. Phys. Chem*. **1982**, *86*, 81.
(15) Lin, C. L. *Int. J. Chem. Kinet*. **1982**, *14*, 593.
(16) Leu, M.-T.; Smith, R. H. *J. Phys. Chem*. **1982**, *86*, 73.
(17) Wine, P. H.; Kreutter, N. M.; Gump, C. A.; Ravishankara, A. R. *J. Phys. Chem*. **1981** *85*, 2660.
(18) Cox, R. A.; Sheppard, D. *Nature* (London) **1980**, *284*, 330.
(19) Perry, R. A.; Atkinson, R.; Pitts, J. N., Jr. *J. Chem. Phys*. **1976**, *64*, 3237.
(20) Stuhl, F. *Ber. Bunsen-Ges. Phys. Chem*. **1974**, *78*, 230.
(21) Westenberg, A. A.; DeHaas, N. *J. Chem. Phys*. **1973**, *59*, 6685.
(22) Frisch, M. J.; Trucks, G. W.; Schlegel, H. B.; Scuseria, G. E.; Robb, M. A.; Cheeseman, J. R.; Zakrzewski, V. G.; Montgomery, J. A., Jr.; Stratmann, R. E.; Burant, J. C.; Dapprich, S.; Millam, J. M.; Daniels, A. D.; Kudin, K. N.; Strain, M. C.; Farkas, O.; Tomasi, J.; Barone, V.; Cossi, M.; Cammi, R.; Mennucci, B.; Pomelli, C.; Adamo, C.; Clifford, S.; Ochterski, J.; Petersson, G. A.; Ayala, P. Y.; Cui, Q.; Morokuma, K.; Malick, D. K.; Rabuck, A. D.; Raghavachari, K.; Foresman, J. B.; Cioslowski, J.; Ortiz, J. V.; Stefanov, B. B.; Liu, G.; Liashenko, A.; Piskorz, P.; Komaromi, I.; Gomperts, R.; Martin, R. L.; Fox, D. J.; Keith, T.; Al-Laham, M. A.; Peng, C. Y.; Nanayakkara, A.; Gonzalez, C.; Challacombe, M.; Gill, P. M. W.; Johnson, B. G.; Chen, W.; Wong, M. W.; Andres, J. L.; Head-Gordon, M.; Replogle, E. S.; Pople, J. A. *Gaussian 98*, revision A.3; Gaussian, Inc.: Pittsburgh, PA, 1998.
(23) Schlegel, H. B. *J. Chem. Phys*. **1986**, *84*, 4530. Sosa, C.; Schlegel, H. B. *Int. J. Quantum Chem*. **1986**, *29*, 1001.
(24) Curtiss, L. A.; Raghavachari, K.; Trucks, G. W.; Pople, J. A. *J. Chem. Phys*. **1991**, *94*, 7221.
(25) Krishnan, R.; Pople, J. A. *Int. J. Quantum Chem*. **1978**, *14*, 91. Krishnan, R.; Frisch, M. J.; Pople, J. A. *J. Chem. Phys*. **1980**, *72*, 4244.
(26) McDouall, J. J.; Peasley, K.; Robb, M. A. *Chem. Phys. Lett*. **1988**, *148*, 183.
(27) Pople, J. A.; Head-Gordon, M.; Raghavachari, K. *J. Chem. Phys*. **1987**, *87*, 5968. Cizek, J. *Adv. Chem. Phys*. **1969**, *14*, 35. Scuseria, G. E.; Schaefer, H. F., III *J. Chem. Phys.* **1989**, *90*, 3700.
(28) Becke, A. D. *J. Chem. Phys*. **1993**, *98*, 5648.
(29) Johnston, H. S. *Gas-Phase Reaction Rate Theory*; Ronald Press: New York, 1966. Laidler, K. J. *Theories of Chemical Reaction Rates*; McGraw-Hill: New York, 1969. Coulson, D. R. *J. Am. Chem. Soc*. **1978**, *100*, 2992.
(30) LeRoy, D. J.; Ridley, B. A.; Quickert, K. A. *Discuss. Faraday Soc*. **1967**, *44*, 92.
(31) Garrett, B. C.; Truhlar, D. G. *J. Am. Chem. Soc*., **1979**, *101*, 4534. Gonzales-Lafont, A.; Truong, T. N.; Truhlar, D. G. *J. Chem. Phys*. **1991**, *95*, 8875. Rice, B. M.; Adams, G. F.; Page, M.; Thompson, D. L. *J. Phys. Chem*. **1995**, *99*, 5016.
(32) (a) Mousavipour, S. H.; Emad, L.; Fakhraee, S. *J. Phys. Chem. A* **2002**, *106*, 2489. (b) Pacey, P. D. *J. Phys. Chem. A* **1998**, *102*, 8541.
(33) Pitzer, K. S. *J. Chem. Phys*. **1946**, *14*, 239.
(34) LeBlance, J. F.; Pacey, P. D. *J. Chem. Phys*. **1985**, *83*, 4511.
(35) Pacey, P. D. *J. Chem. Phys*. **1982**, *77*, 3540.
(36) Pitt, I. G.; Gilbert, G. R.; Ryan, K. R. *J. Phys. Chem*. **1995**, *99*, 239.
(37) Stern, M. J.; Weston, R. E., Jr. *J. Chem. Phys*. **1974**, *60*, 2803, 2808, 2815.
(38) Shavitt, I. *J. Chem. Phys*. **1959**, *31*, 1359.
(39) Eckart, C. *Phys. Rev*. **1930**, *35*, 1303.
(40) Bowdridge, M.; Furue, H.; Pacey, P. D. *J. Phys. Chem*. **1996**, *100*, 1676.
(41) Brown, R. L. *J. Res. Natl. Bur. Stand*. **1981**, *86*, 357.
(42) Furue, H.; Pacey, P. D. *J. Chem. Phys*. **1985**, *83*, 2878.
(43) *Handbook of Chemistry and Physics*, 80th ed.; Lide, D. R., Ed.; CRC Press: Boca Raton, FL, 1999−2000.
(44) Liu, G.-X.; Li, Z.-S.; Xiao, J.-F.; Liu, J.-Y.; Fu, Q.; Huang, X.-R.; Sun, C.-C.; Tang, A.-C. *ChemPhysChem* **2002**, *7*, 625. Fox, G. L.; Schlegel, H. B. *J. Phys. Chem*. **1992**, *96*, 298.
(45) Jacox, M. E. *J. Phys. Chem. Ref. Data* **1994**, Monograph 3.
(46) Shimanouchi, T. *Tables of Molecular Vibrational Frequencies*; NSRDS−NBS-39; American Chemical Society and the American Institute of Physics for the National Bureau of Standards: New York, 1972, Consolidated Vol. 1.
(47) (a) For reaction OH + NH_3, see ref 39. (b) For reaction CH_3 + $(CH_3)_2CO$, see Mousavipour, S. H.; Pacey, P. D. *J. Phys. Chem.* **1996**, *100*, 3573. (c) For CH_3 + H_2, see Furue, H.; Pacey, P. D. *J. Phys. Chem*. **1986**, *90*, 397.
(48) Herschbach, D. R.; Johnston, H. S.; Pitzer, K. S.; Powell, R. E. *J. Chem. Phys*. **1956**, *25*, 736.
(49) Gurvich, L. V.; Veyts, I. V.; Alcock, C. B. *Thermodynamic Properties of Individual Substances*, 4th ed.; Hemisphere Pub. Co.: New York, 1989.
(50) Cox, J. D.; Wagman, D. D.; Medvedev, V. A. *CODATA Key Values for Thermodynamics*; Hemisphere Pub. Co.: New York, 1989.
(51) Corchado, J. C.; Espinosa-Garcia, J.; Hu, W.-P.; Rossi, I.; Truhlar, D. G. *J. Phys. Chem.* **1995**, *99*, 687.